Cavity Controlled Upconversion in CdSe Nanoplatelet Polaritons

Mitesh Amin[1†], Eric R Koessler[2†], Ovishek Morshed[1], Farwa Awan[2], Nicole MB Cogan[2], Robert Collison[1], Trevor M. Tumiel[2], William Girten[2], Christopher S. Leiter[3], A. Nickolas Vamivakas[1,4], Pengfei Huo[2,1*], Todd D. Krauss[2,1*]

[1]The Institute of Optics, University of Rochester, Rochester, NY 14627, USA

[2]Department of Chemistry, University of Rochester, Rochester, NY 14627, USA

[3]Department of Chemistry, Regis University, Denver, CO 80221, USA

[4]Department of Physics and Astronomy, University of Rochester, Rochester, NY 14627, USA

[†]Authors contributed equally to this work.

*Corresponding authors: Pengfei Huo, Todd D. Krauss
Email: pengfei.huo@rochester.edu, todd.krauss@rochester.edu

Abstract

Strong coupling between electronic transitions of matter and confined electromagnetic fields inside an optical cavity creates hybrid, light-matter states known as polaritons. Polaritons provide a versatile platform for investigating quantum electrodynamics effects in chemical systems, such as polariton-altered chemical reactivity. However, using polaritons in chemical contexts will require a better understanding of the photophysical properties of polaritons, especially at ambient temperature and pressure, where chemistry is typically performed. Here, we investigated leveraging strong light-matter interactions to control the excited state dynamics of colloidal CdSe nanoplatelets (NPLs) coupled to a Fabry-Pérot optical cavity. Importantly, changes in the cavity quality (Q) factor, which is a measure of photon loss from the cavity, were used to profoundly change the polariton dynamics. As the Q-factor was increased, we observed significant population of the upper polariton (UP) state, exemplified by the rare observation of substantial UP photoluminescence (PL) at room temperature. In fact, with low energy excitation at the lower polariton (LP), which is not absorbed by uncoupled nanoplatelets, we observed upconverted PL emission from the UP branch, due to efficient exchange of population between the LP, UP and the reservoir of dark states present in collectively coupled polaritonic systems. Critical physical insight into the mechanism of PL enhancement of the UP, and PL upconversion, was provided by state-of-the-art quantum dynamics simulations that account for multiple cavity electromagnetic modes and cavity loss. In addition, by resolving lower and upper polariton PL lifetimes, we found timescales for polariton dynamics on the order of 100 picoseconds, implying great potential for NPL based polariton systems to affect photochemical reaction rates. This work provides important insight into the photophysics of nanocrystal-based exciton-polariton systems and is a significant step towards the development of practical polariton photochemistry platforms.

Introduction

The quantum-mechanical coupling of the electronic states of matter to the electromagnetic modes of an optical cavity results in two new hybrid light-matter eigenstates known as the upper polariton (UP) and lower polariton (LP). For nano-molecular systems (such as colloidal nanocrystals (1, 2)) that have an excitonic photoexcited state, these light-matter eigenstates are termed exciton-polaritons. Recent advances in the field of exciton-polariton systems have led to their proposed use for altering chemical reactivity (3-11), enhancing intermolecular energy transfer (12-15), enabling room temperature Bose-Einstein condensates (16-18), and providing qubits for quantum simulation (19-21). With respect to the specific application of using polaritons for altering chemical reactivity, polaritons are thought to alter frontier molecular orbitals as well as orbital energetics, thus providing the fundamental basis for novel chemical reactivity. For example,

calculations suggest that strong light-molecule coupling can dramatically increase charge transfer rates by a few orders of magnitude, alter electron-phonon coupling, and modify energy landscapes (22-26). Indeed, recent experimental work has shown that strong coupling to the electronic states of photoswitchable molecules can modify the kinetics of their isomerization (10). Strong coupling to the vibrational modes of molecules has led to changes in ground state chemical reactivity, including modifying the distribution of products from a disassociation (27, 28) and the suppression of reaction rates for alcoholysis of phenyl isocyanate with cyclohexanol (11).

While polariton photochemistry provides exciting promise for a new paradigm for chemical transformations, fulfilling that promise will require a thorough understanding of how optical cavities can be used to control polariton photophysics, which is an active area of research. For instance, molecular polaritonic systems often operate in the collective coupling regime, whereby the polariton state is a single, coherent, quantum-mechanical superposition of excitations from thousands to millions of molecules (29). However, this collective coupling also results in a dense manifold of optically inactive exciton states that only weakly couple with the cavity photon (30-32). Having mostly matter (i.e. excitonic) character, this exciton reservoir of dark states dominates the LP and UP dynamics (33-36), leading to the question of whether modified chemical reactivity is even possible under these collective coupling conditions (37-39). Alternatively, for colloidal nanocrystal based polariton systems, which have orders of magnitude fewer emitters coupled to the cavity (40), the influence of the dark state reservoir on the photophysics of the UP and LP is largely unexplored, and thus could provide unique opportunities for nano-molecular polariton systems (38, 41, 42).

In this work, we explore tuning the exciton-polariton photophysics of 2D cadmium selenide (CdSe) nanoplatelets (NPLs) strongly coupled to a high quality (Q)-factor FP optical cavity. By reducing the cavity loss rate, we observed photoluminescence (PL) from the UP state due to efficient population transfer from the reservoir of dark states, as verified by both experiments and quantum dynamical calculations. In fact, in this high-quality cavity, the relatively strong coupling between the UP, LP and dark states allowed for photoexcitation at the LP energy, which normally would not be absorbed by the NPLs, to be upconverted to create a finite population in the UP. The polariton dynamics of these high-Q cavities under ambient conditions led to measured polariton PL lifetimes on the order of 100 picoseconds, which are long enough to provide a fundamental basis for NPL polariton systems to affect photochemical reaction rates.

Results

Polariton Dispersion Characteristics

CdSe NPLs have been recently explored in various exciton-polaritonic systems (43-46) due to their well-defined narrow absorption and photoluminescence (PL) linewidths (~40 meV), high oscillator strengths, and small Stokes shifts (~5-10 meV), making them excellent materials for achieving and investigating strong light-matter coupling (47-50). Here, we integrated 4.5 monolayer CdSe NPLs (approximate lateral size of 22 nm x 15 nm, see SI Appendix for fabrication details**)** into two types of FP microcavities with varying cavity Q-factors as illustrated in Fig. 1A. For FP cavities, the cavity frequency $\omega_{\mathbf{k}}$ depends on the wavevector of the mode and can be expressed as

$$\hbar\omega_{\mathbf{k}} = \hbar\omega_{\mathrm{c}}\sqrt{1+\left(\frac{k_{\parallel}}{k_{\perp}}\right)^{2}} = \hbar\omega_{\mathrm{c}}\sqrt{1+(\tan\theta)^{2}}$$

where $\hbar\omega_{\mathrm{c}} = \frac{\hbar c k_{\perp}}{n}$ is the cavity energy at normal incidence, ***c*** is the speed of light, n is the refractive index inside the cavity, $k_{\parallel}$ and $k_{\perp}$ are the wavevector components of the photon mode which are parallel and perpendicular to the cavity mirrors, respectively, and $\theta = \arctan\left(\frac{k_{\parallel}}{k_{\perp}}\right)$ is the angle of incidence and emission. The perpendicular wavevector component $k_{\perp}$ is fixed and only the parallel component $k_{\parallel}$ will vary as a function of emission angle θ, thus giving rise to the angular dependence (i.e. dispersion) of the cavity mode (SI Appendix, Fig. S3). The Q-factor of a cavity is $\mathrm{Q} = \frac{\omega_{\mathrm{c}}}{\gamma_{\mathrm{c}}}$, where γ_{c} is the bare cavity loss rate. For the higher Q cavity, the heavy hole (HH) absorption transition defined at 2.42 eV (Fig. 1B) is in resonance with the fundamental mode of the 3*λ*/2*n* cavity, where a thin 60 nm NPL film is deposited at the antinode of the cavity having an effective index of refraction *n*. For the lower Q cavity, a thicker 110 nm NPL layer is deposited in resonance with the first order *λ*/2*n* mode cavity.

We hypothesized that increasing the Q-factor of the FP cavity would enable new polariton photophysical behavior, due to the significant effect of cavity loss on polariton population dynamics (51, 52). As illustrated in Fig. 1A, compared to a cavity that is entirely filled with NPLs (53), we calculated that adding inert spacer layers between the NPLs and the mirrors would greatly increase the FP cavity Q-factor. Indeed, adding two 200 nm SiO_2 spacer layers between the NPL layer and the two mirror surfaces provided a Q-factor of approximately 300, compared to a Q-factor of about 70 without the spacers (SI Appendix, Fig. S1). A 31-layer distributed Bragg reflector (DBR) consisting of alternating layers of Si_3N_4 and SiO_2 are used to form the bottom 99.9% reflective

mirror in the 2.25 – 2.75 eV band, while 40 nm of silver deposited on the top spacer layer acts as the top mirror to provide sufficient in and out coupling of light to form the full cavity.

An angle-resolved (Fourier-space) spectroscopy system with a 40X/0.6 NA microscope objective corresponding to a ±19˚collection range (defined by angle inside the active cavity layer) was implemented to measure the cavity angle-resolved reflectance (ARR) and angle-resolved PL (ARPL) spectra. Fig. 1C-D shows the ARR spectra for the two cavities with the NPL HH exciton in resonance with the cavity near zero angle. For the higher Q cavity in Fig. 1D, we see the clear emergence of the two UP and LP absorbing branches split about the uncoupled exciton energy. Both branches of the ARR spectra are fitted with a coupled harmonic oscillator model to extract the Rabi splitting energy in the range of 31 – 45 meV across four detuning energies (SI Appendix, Fig. S3). The detuning energy, Δ, is defined by the energy difference between the cavity resonance at zero angle and the NPL exciton heavy hole transition at 2.42 eV. For the lower Q cavity in Fig. 1C, we observe much broader UP and LP absorbing branches and obtain slightly higher Rabi splitting energies in the range of 50 – 70 meV due to a thicker layer of NPLs.

Corresponding ARPL spectra for all detuning values are taken along various sample positions with 2.56 eV laser excitation. For highly negatively detuned cases (cavity energy less than PL exciton energy, Fig. S3), the PL intensity is exclusively on the LP branch at the angle that corresponds to the NPL-cavity resonance condition. The lack of PL from the UP and the concentration of PL at a small range of collection angles is in agreement with previous NPL-FP polariton systems (40), as well as what has been reported for other exciton-polariton systems (43, 54, 55). However, for the higher Q cavities, as the detuning approaches zero and transitions positive, we observed significant PL emission from the UP branch (in addition to the LP branch) as indicated by the white arrows in Fig. 1D (see also Figure S4). For the blue detuned (Δ = +35 meV) cavity in Fig. S4, a continuum of PL emission can be seen in the ARPL spectra near zero incident angle towards the UP branch. This is in contrast with the lower Q cavity in Fig. 1C where only PL emission from the LP branch is observed. PL emission from the UP branch is exceptionally rare at room temperature, having been reported for only a few polaritonic systems involving organic semiconductors (i.e. *J-aggregated* dyes) (56-59). This rare observation of UP PL is, in part, because the fundamental cavity and exciton properties that affect the full dynamics of the UP, LP and dark state populations, are not well understood.

Physical Origin of Upper Polariton Emission

To better understand the NPL and cavity characteristics that dictate the UP and LP populations as indicated by the measured ARPL spectra, we performed mixed quantum-classical dynamics simulations of the combined NPL-cavity system to calculate the polariton population dynamics and the corresponding PL spectra intensity. The dynamics were propagated using the Lindblad-MASH (L-MASH) method that combines the multi-state mapping approach to surface hopping (MASH) method (60, 61) with Lindblad dynamics (52) to account for cavity loss. The NPL-cavity system was modeled using the generalized Holstein-Tavis-Cummings (GHTC) model, which has been previously used to study light-matter hybrid systems in FP cavities (24, 62, 63). The HTC Hamiltonian includes several phonon-coupled matter excitations coupled to several angle-dependent cavity photon modes, which allows for the calculation of angle-resolved properties of polariton systems including the effect of the reservoir of dark states. The GHTC Hamiltonian can be expressed as

$$H_{GHTC} = H_{NPL} + H_{ph} + H_I$$

Where H_{NPL} describes the exciton states of N independent nanoplatelets, H_{ph} is the Hamiltonian for the quantized cavity mode, and H_I describes the matter-cavity interactions (between H_{NPL} and H_{ph}). The full details of this model can be found in the SI Appendix.

To calculate the angle-resolved PL, the population dynamics of the GHTC model with cavity loss were propagated assuming an incoherent driving of population from an initially populated ground state to the HH states. The steady-state populations arising from this propagation were used to calculate the intensities of the PL spectra shown in Fig. 1C-D by weighting the angle-dependent photonic character of the polariton states by their steady-state populations (62). For both cavities in Fig. 1C-D, the calculated PL spectra shows excellent agreement with experimental spectra both in the shape of the PL dispersion as well as the distribution of intensity as a function of PL energy. In particular for the lower Q = 60 cavity, the calculated PL correctly predicts the emission exclusively from the LP branch near zero angle. For the Q = 300 cavity, the simulations also accurately predict the LP dispersion along with the PL intensity on the UP branch up to around 2.47 eV. For the positive detuning case ($\Delta = +35$ meV) cavity in Fig. S4, the calculated PL also shows good agreement with the measured PL dispersion. These results indicate that the PL spectra obtained from the L-MASH method with the GHTC model can predict experimental PL spectra of these NPL-FP systems with near quantitative accuracy, demonstrating L-MASH as a powerful new simulation tool for such complex polariton systems with cavity loss and many vibrationally-coupled molecules.

The presence of UP PL emission in the simulations can be understood from the perspective of population transfer among a manifold of polariton and dark states. In the simplified picture of strong light-matter coupling (*i.e.* the Tavis-Cummings (TC) model (24)) the optically bright polariton states are completely orthogonal to the large reservoir of dark exciton states (56), and thus they do not exchange excited population. However, more sophisticated treatments (*i.e.* GHTC Hamiltonian) include the influence of phonons coupling to the dark states, which causes them to become energetically disordered and to gain some photonic character (rendering them only quasi-dark). The net result is that the NPL phonons cause a non-adiabatic coupling between the polariton and the quasi-dark states which leads to population transfer among these states over time.

Tuning of Upper Polariton Emission with Q-Factor

We hypothesized that the observance of PL from the UP was primarily due to the higher Q-factor optical cavity, which has less photon loss than is normally found in other polariton systems (25, 64), thereby allowing for a greater chance of populating states with larger photonic character (*i.e*. the higher-angle UP states) before the photon exits the cavity. To investigate this possibility, we simulated polariton PL spectra with different Q-factors (Fig. 1E) for the fixed experimental conditions in Fig. 1D to understand the effect of cavity loss on polariton dynamics. For small Q-factors (Q = 30), the PL intensity is primarily in the LP branch, in agreement with previous measurements of polariton PL for nanomolecular exciton-polaritons (40, 53, 64-68). In contrast, for large Q-factors (Q = 3000) there is even greater PL intensity from the UP relative to the (Q = 300) measurements and simulation. This trend is also observed in the dynamics of the excited populations weighted by photonic character (which are proportional to the emission intensity) (69, 70) in the simulation (Fig. 1F) where the higher Q simulations have larger weighted steady-state populations of UP states.

Our simulations confirm the hypothesis that higher Q factors promote UP emission and allow for further insight into the unique polariton dynamics for high Q-factor optical cavities. In particular, for the higher angles of the UP branch to become populated from the quasi-dark state reservoir, the population must first traverse along a manifold of states with various mixtures of photonic character (which straddle the definition between optically “dark” and “bright” states) (SI Appendix, Fig. S7). The traversing population can only reach the photonic UP branch (*i.e.* successfully upconvert from the dark state reservoir to the UP) if the cavity loss rate experienced by the partially photonic manifold of states is sufficiently small. Thus, the amount of PL emission from states with significant photonic character on the UP should strongly depend on the Q factor of the cavity.

Since phonons drive the upconversion of excited population from the dark states to the UP, we would expect a drastic reduction of the upconverted PL intensity from the UP branch at low temperatures. To that end, ARR and ARPL spectra along two sample positions with similar detuned cavity energies (Δ ~ -1 meV) were collected and compared at 295 K and 100 K (Fig. 2A). Two different cavity sample positions were chosen for comparison to account for the temperature dependent HH exciton blue-shift from 2.42 eV to 2.46 eV (SI Appendix, Fig. S8) (71, 72). At 100 K, PL emission is observed solely from the LP branch for small incident angles (± 7˚), in direct contrast to the enhanced UP PL emission out to higher angles (± 12˚) for measurements taken at 295 K.

This reduction in UP emission at lower temperatures was supported by simulations of polariton population dynamics performed at 100 K and 295 K. Indeed, the weighted populations of the UP states (Fig. 2B) were roughly 10-fold smaller in the 100 K simulation versus the simulation at 295 K. This significant difference in UP populations can be explained by the difference in non-adiabatic coupling magnitude between the polariton states at different temperatures. To visualize this difference, in Fig. 2C we plot the energies of the polariton states through time for a cavity mode near 8 degrees off vertical. The different colors in Fig. 2C show the magnitude of non-adiabatic coupling that each polariton state experiences due to the exchange of character between exciton and photon. Since most of the photonic character of this 8 degree cavity mode is shared among UP polariton states, larger values of coupling indicate faster population transfer to these UP states. The UP states in the 295 K simulation experience over twice the amount of non-adiabatic coupling magnitude as those in the 100 K simulation thus the population is transferred more quickly in the UP at room temperature. This faster population transfer rate allows for population to move further uphill along the UP branch at 295 K before cavity loss can significantly deplete it, while at 100 K, the cavity loss depletes the UP population before it can move further uphill along the UP branch.

Polariton Upconversion Enabled by High Q-factor Cavity

A central premise motivating the study of polaritons for novel chemical transformations is that the polariton state has fundamentally different physical properties compared to the purely electronic states of matter (24). For example, predictions that strong light-matter coupling can be leveraged to enable charge transfer to energetically forbidden molecular acceptors rely on relatively efficient population transfer between the LP, UP and the dark states (23). To test the limits of polaritonic population transfer in our system, we resonantly excited the LP branch (2.3 – 2.41 eV) for three different cavity detuned sample positions (SI Appendix, Fig. S9) having similar Rabi splitting energies in the range of 45-49 meV. In the absence of strong coupling between the HH NPL exciton and the cavity, light at these wavelengths does not have enough energy to span the NPL bandgap, and thus is not expected to be absorbed. However, upon excitation of the LP branch

in all three cases, we observed anti-Stokes, PL upconversion to the UP branch as illustrated for the Δ = -52 meV case in Fig. 3A. The upconverted PL dispersion is identical to what was observed when the HH exciton state was populated via high energy photoexcitation, for all detuning values (SI Appendix, Fig. S10). This emergence of UP emission upon LP excitation clearly shows the effectiveness of population transfer from the LP to UP via phonon-mediated interactions with the dark states.

Angle-integrated linecuts along the ARPL spectra reveal that the upconverted PL intensity is enhanced in the polariton system as high as 9-fold for the highly negatively detuned case compared to a control half cavity thin film NPL sample, as shown in Fig. 3B. To approximate similar laser excitation fluence for both samples, the control sample was excited using 1% of the incident power excitation compared to the cavity samples to account for the 99% cavity reflectivity in the 2.3-2.41 eV range. Additionally, we observe a decreasing near-linear dependence in the overall upconversion PL intensity as the cavity is more positively detuned. We attribute this intensity decrease to less available LP states as the cavity is positively detuned, reducing the total amount of absorbed excitation light. The order of magnitude increase in upconverted PL emission (and associated UP excited population) clearly exemplifies how tuning the cavity Q-factor can be used as a powerful tool to control polariton photophysical dynamics.

Polariton Photoluminescence Lifetimes

The simplest picture characterizes the polariton lifetime as a superposition of the radiative rates of the matter and photonic characters of the polariton weighted by the Hopfield coefficients (73). Thus, the polariton has a lifetime bounded by the photon lifetime in the cavity (lower bound) and the uncoupled NPL exciton lifetime (upper bound). However, this idealized picture does not account for polariton coupling to the dark states reservoir, leading to measured lifetimes in collective-coupled exciton-polariton systems equal to or even longer than the uncoupled exciton lifetime (35, 73-77).

To better understand polariton lifetimes from the NPL-FP cavity system with a large Q-factor, we performed high temporal and wavelength resolved time correlated single photon counting (TCSPC) measurements with a dual exit port spectrometer as shown in Fig. 4A. By using the ARR and ARPL spectra (Fig. 4B) as a reference, TCSPC data (Fig. 4C) at a given PL wavelength could be collected with 2-nm resolution through diffraction of the cavity PL emission (SI Appendix, Fig. S13-14). Fig. 4D shows average polariton PL lifetimes resolved across the UPB/LPB for a sample with cavity detuning energy -2 meV, and with a Rabi splitting energy of 47 meV (SI Appendix, Fig. S11). Interestingly, the average polariton PL lifetime appears to reach a minimum of approximately

100 ps when the HH NPL exciton is resonant with the cavity and increases for UP and LP emission energies as the collection angle increases. A similar trend of increasing lifetime towards the higher UP and lower LP emission energies is measured for a highly red detuning energy of -67 meV (SI Appendix, Fig. S15). Additionally, the amplitude-weighted polariton PL lifetimes are on average 1.5-2X times shorter than for the bare thin film samples (188 ps). Our results clearly indicate that the polariton PL lifetimes are not simply weighted by the Hopfield coefficients, which, for example, would result in a cavity photon lifetime of ~ 160 fs near resonant angles corresponding to equal 50% excitonic and 50% photonic characters. Instead, the overall polariton PL lifetimes are significantly prolonged due to continuous population mixing with the dark state reservoir. Nonetheless, the range of measured polariton PL lifetimes (100 – 160 ps) suggests that the transfer of population between the dark and polaritonic states has a dependence on the relative photonic versus excitonic character of the polariton at a given collection angle.

Identifying and comparing the individual PL lifetime components of the polariton and the uncoupled NPL exciton allows for further insight into how strong light-matter coupling affects NPL photophysics. The TCSPC data was fit to a triple exponential with (on average) the shortest lifetime component (t_1 ~ 30 ps) for thin films reduced to 18 ps (~65% decrease) under strong coupling (SI Appendix, Fig. S15). This large change in the short component largely accounts for the average polariton PL lifetime being 1.5-2 times shorter than the uncoupled exciton lifetime, as the medium (t_2 ~ 186 ps) and long (t_3 ~ 1.5 ns) lifetime components remain largely unchanged. The decrease of t_1 inside the cavity can be understood as a consequence of the moderately large number of coupled NPLs (~16,000) which is large enough for the dark states to serve as a population reservoir for the polariton states, yet small enough to allow for an appreciable rate of transfer from these dark reservoir states to the polariton states. This appreciable reservoir to polariton transfer rate in NPL-cavity systems serves as an extra decay channel for the reservoir states, which adds onto the bare non-radiative decay rate to cause a decrease of the lifetime of the reservoir states. This decrease in reservoir lifetime is detected from the UP and LP due to a decrease in the population transfer rate from the reservoir to these polariton states as the reservoir population decays through time. This stands in contrast to many organic polariton systems which can have orders of magnitude more coupled molecules, which greatly reduces the rate of transfer from reservoir to polariton states (29), and consequentially do not have measurably different polariton PL lifetimes compared to the bare organic molecules (35, 74-76). The trend of increasing UP PL lifetime as a function of energy in both Fig. 4D and Fig. S15 also stands in contrast to previous works which found no polariton PL lifetime dependence on energy (35, 73). While higher temporal and energy resolved pump-probe measurements are needed to track the population transfer rates between the individual states, one possible explanation of the trend is that the reduction of non-adiabatic coupling at higher angles

and energies reduces the rate of population lost to other polariton states and thus increases the perceived PL lifetime of those higher energy states.

Discussion

By designing a high Q-factor FP cavity embedded with colloidal 2D CdSe NPLs, we were able to obtain great insight into how cavity parameters can be used to control excited polariton dynamics. Notably, while vibronic coupling allows for excited population to be upconverted from the LP through the dark states to the UP, high Q-factor cavities enable PL emission from the UP branch due to lower photon loss rates among both the UP states and the partially-photonic quasi-dark states. Further, quantum dynamics simulations suggest that that even higher Q cavities at room temperature will allow for a further enhancement of the UP population. The ability to control the upconversion of excited population from LP and dark states to the UP is a significant step toward enhancing forbidden photochemical reaction rates using strong light-matter coupling. For example, a photochemical reaction that has an uphill driving force outside the cavity, and this is nominally forbidden (at equilibrium), could have its reaction rate significantly increased through coupling the molecular donor state to the cavity mode (23, 78).

In addition to controlling polariton excited populations, high Q-factor cavities allowed for measurements of PL lifetimes across the UP and LP states with energy resolved TCSPC. Comparing to average lifetimes of half-cavity NPL films (~188 ps), we see an averaged PL lifetime of ~ 100 ps across two different cavity detuned samples primarily due to a decrease in the polariton short component lifetime, indicating a rapid exchange of population from the dark states to both the UP and LP via phonon coupling. The finding of a polariton lifetime for NPLs different from the free exciton lifetime is atypical for organic polariton systems but expected for these NPL polariton systems with fewer coupled emitters. This has important and direct implications for applications of polaritons in chemical systems. The presence of a finite UP population lasting over 100 picoseconds via uphill transfer from the dark states reservoir demonstrates the potential of polariton systems to affect chemical transformations on this timescale. Indeed, since many photochemical reactions occur on similar or shorter timescales (79, 80) polaritons could participate in such photochemical reactions before dissipation. Altogether, the design of optical cavities that facilitate strong light-matter interactions with large Q-factors is a promising route to enable new chemical transformations with nanocrystal-based polariton systems.

Materials and Methods

Synthesis of 4.5 Monolayer CdSe Nanoplatelets

The synthesis of 4.5 monolayer CdSe nanoplatelets was carried out using a previously reported method (81) with slight modifications. 180 mg of anhydrous cadmium myristate, 30 mg of selenium powder, and 15 mL of 1-octadecene were added in a 100 mL 3-neck round bottom flask. The contents of the flask were degassed at room temperature followed by degassing at 120^{o} C for 60 minutes. The mixture was then returned to a nitrogen environment and the temperature was set to 240^{o} C. At 210^{o} C, the septum was removed from one neck, and 100 mg of cadmium acetate dihydrate were swiftly added to the solution. Once the temperature reached 240^{o} C, it was carefully maintained for 8 minutes. After which the reaction was quickly quenched with the aid of a heat gun followed by a water bath at 190^{o} C. 2 mL of oleic acid was injected at 160^{o} C followed by injection of 15 mL of hexanes at room temperature. The nanoplatelets were precipitated by centrifugation at 3000 rpm for 10 minutes and were redispersed in 12 mL of hexanes. The solution was then allowed to sit overnight followed by centrifugation at 6000 rpm for 15 minutes. The pellet was discarded and the nanoplatelets were kept in an air sealed glass vial.

Microcavity Fabrication

The DBR mirror of the dielectric-metal microcavity was deposited via PE-CVD on Si substrates (1 cm x 1 cm) with 15.5 bilayers of alternating 60 nm Si_3N_4 / 85 nm SiO_2 to form a 99.9% Bragg-reflector in the 450 – 550 nm region. For the bottom spacer layer, 200 nm of SiO_2 was deposited via e-beam PVD or 200 nm of PMMA resist was spin coated onto the DBR mirror – both resulting in similar cavity performance. Concentrated and purified solution of 4.5 ML CdSe NPLs in hexane was drop-casted onto the spacer layer to approximately form a smooth 60 nm nanocrystal film. Another spacer layer of 200 nm SiO_2 and the top 40 nm silver mirror were deposited via e-beam PVD to form the full 3λ/2n Fabry-Pérot microcavity.

Angle Resolved Spectroscopy

For angle resolved spectra measurements, the cavity sample was mounted onto a NanoH100 XY piezo stage (for raster scanning) that is integrated onto an epifluorescence microscope (Nikon TE-2000U). The sample was illuminated through the top silver mirror with an approximate focused 1 um spot size using a 40x/0.6 NA objective (Nikon). Cavity emission was collected from the same objective with dichroic mirrors and the back focal plane of the objective was relayed to the spectrometer with a tube lens for momentum or angle resolved spectra. For cold-temperature measurements, the sample was placed in a Montana Instruments CA50 cryostat with a 60x/0.7 NA

objective. A broadband (450-750 nm) white light LED (Thorlabs) was used for all reflectance spectra and several different laser pump sources were used for collecting angle resolved photoluminescence spectra across multiple experimental setups. A 5 MHz pulsed 485 nm laser diode (PicoQuant LDH-D 485) was used for steady-state room temperature spectra, while a CW 405 nm diode (PicoQuant LDH-D 405) was used for 100 K measurements. For upconversion experiments, a 2.5 MHz pulsed white-light continuum laser (FYLA Iceblink) with a band pass filter was used for a broad 515-540 nm excitation of the LPB.

Lifetime Measurements

A frequency-doubled Ti:sapphire laser (Coherent Mira-900) operating at 410 nm with 76 MHz repetition rate and < 2 ps pulse durations was used for TCSPC lifetime measurements. An Acton SP-2500i dual exit port spectrometer (as shown in Fig. 4A) was used to correlate the angle resolved spectra taken on the CCD with the wavelength-resolved lifetime collection taken with the single-photon APD function (Micro Photon Devices MPD) connected to PicoHarp 300 (PicoQuant) time tagging (4 ps binning) electronics. The spectrometer grating (150 g/mm) along with the exit slits was used to obtain 2 nm wavelength resolution. Lifetime components were obtained by deconvoluting the APD-limited 60 ps instrument response from the individual curves (SI Appendix, Fig. S11-S13) and fitted to a triple exponential function using the open-source MATLAB DecayFit (FluorTools) software. Lifetimes of three random positions along a half-cavity bare NPL film were also measured to compare against the polariton lifetimes.

Quantum Dynamics Simulations

The GHTC Hamiltonian used for simulating the NPL-cavity system modeled $N = 160$ NPL molecules coupled to 40 cavity modes uniformly distributed among the in-plane wavevector component. The steady-state of the populations from the L-MASH propagation were selected after 2 ps of continuous, incoherent driving of the ground state to the HH states with a per-molecule pump intensity of $6/N$ meV. The numerical timestep was $dt = 0.5$ fs and the PL spectra was averaged over 10,000 trajectories. The full details of the model and PL calculations can be found in the SI.

Acknowledgements

Cavity fabrication and characterization was supported by the National Science Foundation “Center for Quantum Electrodynamics for Selective Transformations (QuEST)” under Grant CHE-2124398. Dynamics measurements were supported by the Department of Energy under Grant No. DE-SC0022171. DBR mirrors were fabricated at the Cornell NanoScale Facility (CNF), an NNCI member supported by NSF Grant NNCI-2025233. The authors also acknowledge the support from

Integrated Nanosystems Center (URnano) at the University of Rochester for nanofabrication facilities. Computing resources were provided by the Center for Integrated Research Computing (CIRC) at the University of Rochester. ERK appreciates valuable discussions with Johan Runeson on the MASH method.

References

1. A. L. Efros, L. E. Brus, Nanocrystal Quantum Dots: From Discovery to Modern Development. *ACS Nano* **15**, 6192-6210 (2021).
2. C. B. Murray, C. R. Kagan, M. G. Bawendi, Synthesis and Characterization of Monodisperse Nanocrystals and Close-Packed Nanocrystal Assemblies. *Annual Review of Materials Science* **30**, 545-610 (2000).
3. T. Schwartz, J. A. Hutchison, C. Genet, T. W. Ebbesen, Reversible Switching of Ultrastrong Light-Molecule Coupling. *Physical Review Letters* **106**, 196405 (2011).
4. M. Kowalewski, S. Mukamel, Manipulating molecules with quantum light. *Proceedings of the National Academy of Sciences* **114**, 3278-3280 (2017).
5. B. Munkhbat, M. Wersäll, D. G. Baranov, T. J. Antosiewicz, T. Shegai, Suppression of photo-oxidation of organic chromophores by strong coupling to plasmonic nanoantennas. *Science Advances* **4**, eaas9552.
6. K. Stranius, M. Hertzog, K. Börjesson, Selective manipulation of electronically excited states through strong light–matter interactions. *Nature Communications* **9**, 2273 (2018).
7. A. Mandal, P. Huo, Investigating New Reactivities Enabled by Polariton Photochemistry. *The Journal of Physical Chemistry Letters* **10**, 5519-5529 (2019).
8. J. Feist, J. Galego, F. J. Garcia-Vidal, Polaritonic Chemistry with Organic Molecules. *ACS Photonics* **5**, 205-216 (2018).
9. R. F. Ribeiro, L. A. Martínez-Martínez, M. Du, J. Campos-Gonzalez-Angulo, J. Yuen-Zhou, Polariton chemistry: controlling molecular dynamics with optical cavities. *Chemical Science* **9**, 6325-6339 (2018).
10. H. Zeng *et al.*, Control of Photoswitching Kinetics with Strong Light–Matter Coupling in a Cavity. *Journal of the American Chemical Society* **145**, 19655-19661 (2023).
11. W. Ahn, J. F. Triana, F. Recabal, F. Herrera, B. S. Simpkins, Modification of ground-state chemical reactivity via light–matter coherence in infrared cavities. *Science* **380**, 1165-1168 (2023).
12. K. Georgiou, R. Jayaprakash, A. Othonos, D. G. Lidzey, Ultralong-Range Polariton-Assisted Energy Transfer in Organic Microcavities. *Angewandte Chemie International Edition* **60**, 16661-16667 (2021).
13. D. M. Coles *et al.*, Polariton-mediated energy transfer between organic dyes in a strongly coupled optical microcavity. *Nature Materials* **13**, 712-719 (2014).
14. R. F. Ribeiro, Multimode polariton effects on molecular energy transport and spectral fluctuations. *Communications Chemistry* **5**, 48 (2022).
15. D. Xu *et al.*, Ultrafast imaging of polariton propagation and interactions. *Nature Communications* **14**, 3881 (2023).
16. J. Kasprzak *et al.*, Bose–Einstein condensation of exciton polaritons. *Nature* **443**, 409-414 (2006).
17. H. Deng, H. Haug, Y. Yamamoto, Exciton-polariton Bose-Einstein condensation. *Reviews of Modern Physics* **82**, 1489-1537 (2010).
18. J. D. Plumhof, T. Stöferle, L. Mai, U. Scherf, R. F. Mahrt, Room-temperature Bose–Einstein condensation of cavity exciton–polaritons in a polymer. *Nature Materials* **13**, 247-252 (2014).
19. S. Ghosh, T. C. H. Liew, Quantum computing with exciton-polariton condensates. *npj Quantum Information* **6**, 16 (2020).

20. N. Y. Kim, Y. Yamamoto, "Exciton-Polariton Quantum Simulators" in Quantum Simulations with Photons and Polaritons: Merging Quantum Optics with Condensed Matter Physics, D. G. Angelakis, Ed. (Springer International Publishing, Cham, 2017), 10.1007/978-3-319-52025-4_5, pp. 91-121.
21. T. Boulier *et al.*, Microcavity Polaritons for Quantum Simulation. *Advanced Quantum Technologies* **3**, 2000052 (2020).
22. J. A. Hutchison, T. Schwartz, C. Genet, E. Devaux, T. W. Ebbesen, Modifying Chemical Landscapes by Coupling to Vacuum Fields. *Angewandte Chemie International Edition* **51**, 1592-1596 (2012).
23. A. Mandal, T. D. Krauss, P. Huo, Polariton-Mediated Electron Transfer via Cavity Quantum Electrodynamics. *The Journal of Physical Chemistry B* **124**, 6321-6340 (2020).
24. A. Mandal *et al.*, Theoretical Advances in Polariton Chemistry and Molecular Cavity Quantum Electrodynamics. *Chemical Reviews* **123**, 9786-9879 (2023).
25. R. Bhuyan *et al.*, The Rise and Current Status of Polaritonic Photochemistry and Photophysics. *Chemical Reviews* **123**, 10877-10919 (2023).
26. B. M. Weight, T. D. Krauss, P. Huo, Investigating Molecular Exciton Polaritons Using Ab Initio Cavity Quantum Electrodynamics. *The Journal of Physical Chemistry Letters* **14**, 5901-5913 (2023).
27. A. Thomas *et al.*, Tilting a ground-state reactivity landscape by vibrational strong coupling. *Science* **363**, 615-619 (2019).
28. F. J. Garcia-Vidal, C. Ciuti, T. W. Ebbesen, Manipulating matter by strong coupling to vacuum fields. *Science* **373**, eabd0336 (2021).
29. J. d. Pino, J. Feist, F. J. Garcia-Vidal, Quantum theory of collective strong coupling of molecular vibrations with a microcavity mode. *New Journal of Physics* **17**, 053040 (2015).
30. M. Litinskaya, P. Reineker, V. M. Agranovich, Fast polariton relaxation in strongly coupled organic microcavities. *Journal of Luminescence* **110**, 364-372 (2004).
31. M. Tavis, F. W. Cummings, The exact solution of N two level systems interacting with a single mode, quantized radiation field. *Physics Letters A* **25**, 714-715 (1967).
32. M. Tavis, F. W. Cummings, Exact Solution for an N-Molecule---Radiation-Field Hamiltonian. *Physical Review* **170**, 379-384 (1968).
33. F. Fassioli, K. H. Park, S. E. Bard, G. D. Scholes, Femtosecond Photophysics of Molecular Polaritons. *The Journal of Physical Chemistry Letters* **12**, 11444-11459 (2021).
34. G. D. Scholes, C. A. DelPo, B. Kudisch, Entropy Reorders Polariton States. *The Journal of Physical Chemistry Letters* **11**, 6389-6395 (2020).
35. B. Xiang *et al.*, State-Selective Polariton to Dark State Relaxation Dynamics. *The Journal of Physical Chemistry A* **123**, 5918-5927 (2019).
36. T. Khazanov *et al.*, Embrace the darkness: An experimental perspective on organic exciton–polaritons. *Chemical Physics Reviews* **4**, 041305 (2023).
37. E. Michail *et al.*, Addressing the Dark State Problem in Strongly Coupled Organic Exciton-Polariton Systems. *Nano Letters* **24**, 557-565 (2024).
38. B. Liu, V. M. Menon, M. Y. Sfeir, The Role of Long-Lived Excitons in the Dynamics of Strongly Coupled Molecular Polaritons. *ACS Photonics* **7**, 2292-2301 (2020).
39. G. Groenhof, C. Climent, J. Feist, D. Morozov, J. J. Toppari, Tracking Polariton Relaxation with Multiscale Molecular Dynamics Simulations. *The Journal of Physical Chemistry Letters* **10**, 5476-5483 (2019).
40. L. Qiu *et al.*, Molecular Polaritons Generated from Strong Coupling between CdSe Nanoplatelets and a Dielectric Optical Cavity. *The Journal of Physical Chemistry Letters* **12**, 5030-5038 (2021).
41. M. Du, J. A. Campos-Gonzalez-Angulo, J. Yuen-Zhou, Nonequilibrium effects of cavity leakage and vibrational dissipation in thermally activated polariton chemistry. *The Journal of Chemical Physics* **154**, 084108 (2021).
42. A. Koner, M. Du, S. Pannir-Sivajothi, R. H. Goldsmith, J. Yuen-Zhou, A path towards single molecule vibrational strong coupling in a Fabry–Pérot microcavity. *Chemical Science* **14**, 7753-7761 (2023).

43. L. C. Flatten *et al.*, Strong Exciton–Photon Coupling with Colloidal Nanoplatelets in an Open Microcavity. *Nano Letters* **16**, 7137-7141 (2016).
44. J. M. Winkler *et al.*, Room-Temperature Strong Coupling of CdSe Nanoplatelets and Plasmonic Hole Arrays. *Nano Letters* **19**, 108-115 (2019).
45. I. Shlesinger *et al.*, Strong Coupling of Nanoplatelets and Surface Plasmons on a Gold Surface. *ACS Photonics* **6**, 2643-2648 (2019).
46. H. Yang *et al.*, Ultralow Threshold Room Temperature Polariton Condensation in Colloidal CdSe/CdS Core/Shell Nanoplatelets. *Advanced Science* **9**, 2200395 (2022).
47. S. Ithurria *et al.*, Colloidal nanoplatelets with two-dimensional electronic structure. *Nature Materials* **10**, 936-941 (2011).
48. M. D. Tessier, C. Javaux, I. Maksimovic, V. Loriette, B. Dubertret, Spectroscopy of Single CdSe Nanoplatelets. *ACS Nano* **6**, 6751-6758 (2012).
49. P. Geiregat *et al.*, Localization-limited exciton oscillator strength in colloidal CdSe nanoplatelets revealed by the optically induced stark effect. *Light: Science & Applications* **10**, 112 (2021).
50. S. Ithurria, B. Dubertret, Quasi 2D Colloidal CdSe Platelets with Thicknesses Controlled at the Atomic Level. *Journal of the American Chemical Society* **130**, 16504-16505 (2008).
51. R. Pandya *et al.*, Tuning the Coherent Propagation of Organic Exciton-Polaritons through Dark State Delocalization. *Advanced Science* **9**, 2105569 (2022).
52. E. R. Koessler, A. Mandal, P. Huo, Incorporating Lindblad decay dynamics into mixed quantum-classical simulations. *The Journal of Chemical Physics* **157**, 064101 (2022).
53. M. A. Ovishek Morshed, Rob Collison, Nicole MB Cogan, Eric R Koessler, Trevor M Tumiel, William Girten, Farwa Awan, Lele Mathis, Pengfei Huo, A Nickolas Vamivakas, Teri W Odom, Todd D Krauss, Room-Temperature Strong Coupling between CdSe Nanoplatelets and a Metal-DBR Fabry-Perot Cavity. *ChemRxiv* 10.26434/chemrxiv-2023-9kllm (2023).
54. T. Neuman, J. Aizpurua, Origin of the asymmetric light emission from molecular exciton–polaritons. *Optica* **5**, 1247-1255 (2018).
55. K. Müller *et al.*, Ultrafast Polariton-Phonon Dynamics of Strongly Coupled Quantum Dot-Nanocavity Systems. *Physical Review X* **5**, 031006 (2015).
56. D. M. Coles, P. Michetti, C. Clark, A. M. Adawi, D. G. Lidzey, Temperature dependence of the upper-branch polariton population in an organic semiconductor microcavity. *Physical Review B* **84**, 205214 (2011).
57. D. G. Lidzey *et al.*, Experimental study of light emission from strongly coupled organic semiconductor microcavities following nonresonant laser excitation. *Physical Review B* **65**, 195312 (2002).
58. P. Michetti, G. C. La Rocca, Simulation of J-aggregate microcavity photoluminescence. *Physical Review B* **77**, 195301 (2008).
59. J. Wenus, L. G. Connolly, D. G. Lidzey, New organic materials and microcavity structures for strong exciton-photon coupling. *physica status solidi (c)* **2**, 3899-3902 (2005).
60. J. R. Mannouch, J. O. Richardson, A mapping approach to surface hopping. *The Journal of Chemical Physics* **158**, 104111 (2023).
61. J. E. Runeson, D. E. Manolopoulos, A multi-state mapping approach to surface hopping. *The Journal of Chemical Physics* **159**, 094115 (2023).
62. R. H. Tichauer, J. Feist, G. Groenhof, Multi-scale dynamics simulations of molecular polaritons: The effect of multiple cavity modes on polariton relaxation. *The Journal of Chemical Physics* **154**, 104112 (2021).
63. Q. Zhang, K. Zhang, Collective effects of organic molecules based on the Holstein–Tavis–Cummings model. *Journal of Physics B: Atomic, Molecular and Optical Physics* **54**, 145101 (2021).
64. P. A. Hobson *et al.*, Strong exciton–photon coupling in a low-Q all-metal mirror microcavity. *Applied Physics Letters* **81**, 3519-3521 (2002).
65. D. G. Lidzey *et al.*, Room Temperature Polariton Emission from Strongly Coupled Organic Semiconductor Microcavities. *Physical Review Letters* **82**, 3316-3319 (1999).

66. S. Kéna-Cohen, S. R. Forrest, Green polariton photoluminescence using the red-emitting phosphor PtOEP. *Physical Review B* **76**, 075202 (2007).
67. D. Ballarini *et al.*, Polariton-Induced Enhanced Emission from an Organic Dye under the Strong Coupling Regime. *Advanced Optical Materials* **2**, 1076-1081 (2014).
68. D. M. Coles, R. T. Grant, D. G. Lidzey, C. Clark, P. G. Lagoudakis, Imaging the polariton relaxation bottleneck in strongly coupled organic semiconductor microcavities. *Physical Review B* **88**, 121303 (2013).
69. F. Herrera, F. C. Spano, Absorption and photoluminescence in organic cavity QED. *Physical Review A* **95**, 053867 (2017).
70. D. G. Lidzey, D. D. C. Bradley, A. Armitage, S. Walker, M. S. Skolnick, Photon-Mediated Hybridization of Frenkel Excitons in Organic Semiconductor Microcavities. *Science* **288**, 1620-1623 (2000).
71. Y. P. Varshni, Temperature dependence of the energy gap in semiconductors. *Physica* **34**, 149-154 (1967).
72. A. Al Salman *et al.*, Temperature effects on the spectral properties of colloidal CdSe nanodots, nanorods, and tetrapods. *Applied Physics Letters* **90**, 093104 (2007).
73. J. Mony, M. Hertzog, K. Kushwaha, K. Börjesson, Angle-Independent Polariton Emission Lifetime Shown by Perylene Hybridized to the Vacuum Field Inside a Fabry–Pérot Cavity. *The Journal of Physical Chemistry C* **122**, 24917-24923 (2018).
74. T. Schwartz *et al.*, Polariton Dynamics under Strong Light–Molecule Coupling. *ChemPhysChem* **14**, 125-131 (2013).
75. S. Wang *et al.*, Quantum Yield of Polariton Emission from Hybrid Light-Matter States. *The Journal of Physical Chemistry Letters* **5**, 1433-1439 (2014).
76. A. Canaguier-Durand, C. Genet, A. Lambrecht, T. W. Ebbesen, S. Reynaud, Non-Markovian polariton dynamics in organic strong coupling. *The European Physical Journal D* **69**, 24 (2015).
77. M. Laitz *et al.*, Uncovering temperature-dependent exciton-polariton relaxation mechanisms in hybrid organic-inorganic perovskites. *Nature Communications* **14**, 2426 (2023).
78. L. Mauro, K. Caicedo, G. Jonusauskas, R. Avriller, Charge-transfer chemical reactions in nanofluidic Fabry-P\'erot cavities. *Physical Review B* **103**, 165412 (2021).
79. J.-Y. Xu *et al.*, Ultrafast Dynamics of Charge Transfer and Photochemical Reactions in Solar Energy Conversion. *Advanced Science* **5**, 1800221 (2018).
80. K. R. Gopidas, M. Bohorquez, P. V. Kamat, Photophysical and photochemical aspects of coupled semiconductors: charge-transfer processes in colloidal cadmium sulfide-titania and cadmium sulfide-silver(I) iodide systems. *The Journal of Physical Chemistry* **94**, 6435-6440 (1990).
81. G. H. V. Bertrand, A. Polovitsyn, S. Christodoulou, A. H. Khan, I. Moreels, Shape control of zincblende CdSe nanoplatelets. *Chemical Communications* **52**, 11975-11978 (2016).

Figures

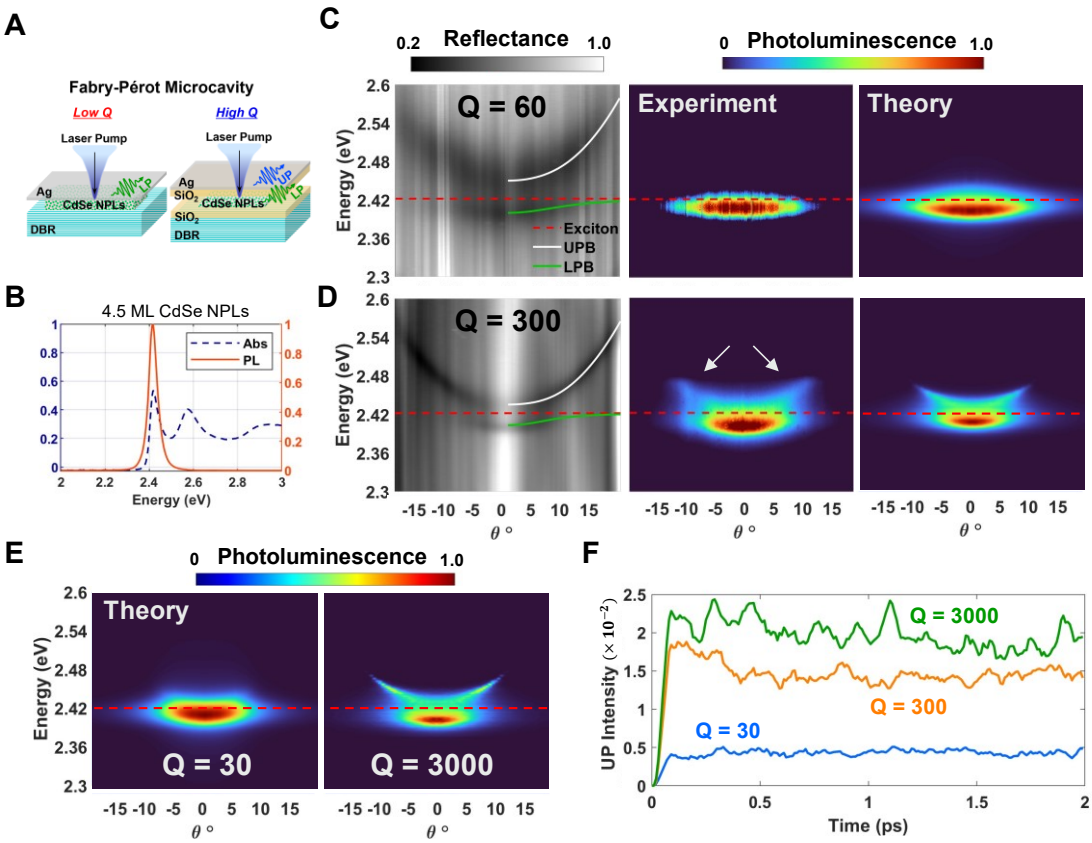

Figure 1. Strong coupling of CdSe NPLs in a microcavity at room temperature. (A) Metal-dielectric DBR cavity geometry for a lower cavity quality factor $Q = 60$ and for a higher $Q = 300$ with SiO_2 spacers. **(B)** Absorbance (dotted blue) and PL (red) of 4.5 ML CdSe NPLs in solution. **(C)** Angle-resolved reflectance (left) & PL spectra (experimental middle, simulated right) with fitted UPB (white), LPB (green), and exciton heavy-hole transition energy at 2.42 eV (dotted red) overlay for a sample corresponding to detuning energy $\Delta = +6\,meV$, Rabi-splitting energy $\hbar\Omega_R = 50\,meV$, and $Q = 60$. **(D)** Same as (C) but with $\Delta = -1\,meV$, $\hbar\Omega_R = 31\,meV$, $Q = 300$. Corresponding simulated quantum dynamical simulations showing excellent agreement with measured spectra with white arrows indicating UPB PL emission. **(E)** Simulated ARPL spectra for varying Q-factor or cavity loss rates for experimental conditions in (D). **(F)** Theoretical calculations of the UP populations above 2.437 eV weighted by photonic character (which is proportional to emission intensity), indicating greater UPB population buildup for increasing cavity Q-factor.

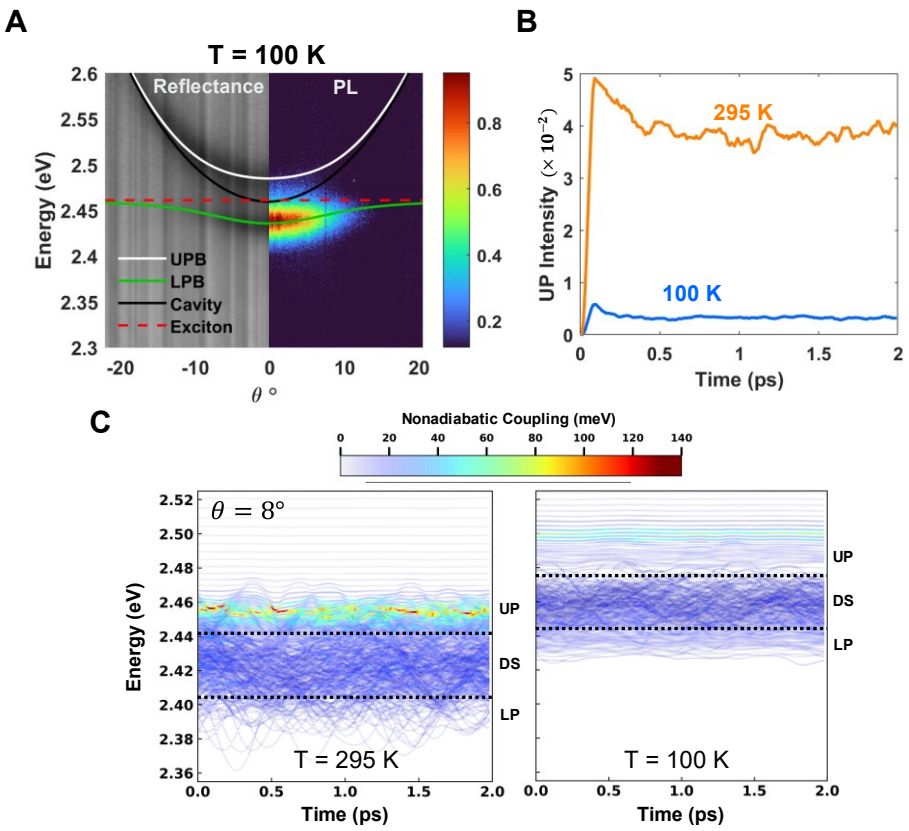

Figure 2. Upper Polariton State Populations at 295 K vs. 100 K. (A) Angle-resolved reflectance and PL spectra taken at 100 K for near resonant detuning of $\Delta = -1\ meV$, $\hbar\Omega_R = 49\ meV$ with fitted polariton branches showing suppressed UP PL emission. **(B)** Theoretical calculations of the UP populations above the HH exciton energy weighted by photonic character, indicating greater UPB emission at 295 K versus 100 K. **(C)** Polariton state energies through time of an arbitrary trajectory colored by the magnitude of non-adiabatic coupling due to exchange of character of the cavity mode near 8 degrees, indicating larger UP population transfer rates at 295 K versus 100 K (see SI for full non-adiabatic coupling expression). In the simulation, the orange and red regions of the plot correspond to larger coupling values, which promote population transfer from the dark states (DS) to the UP.

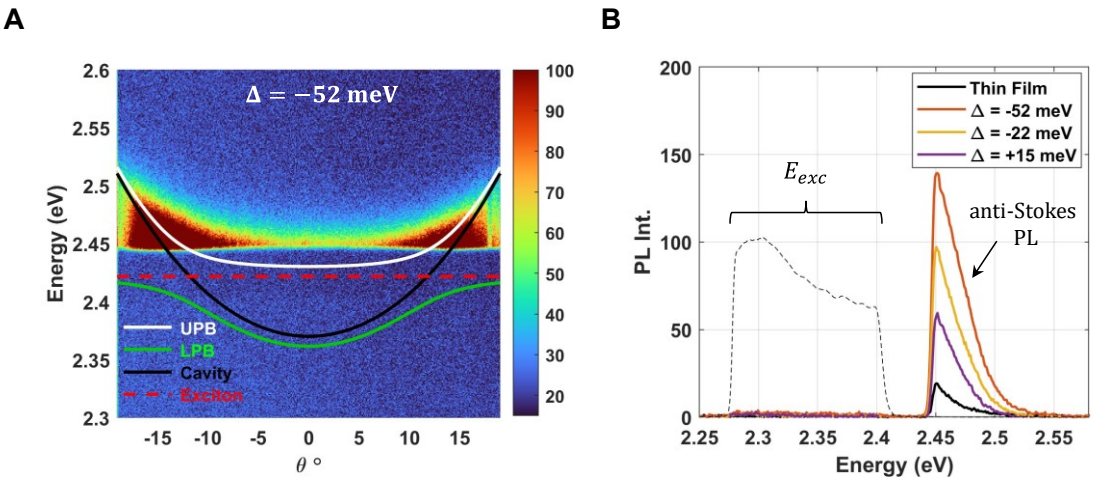

Figure 3. PL upconversion and emission from the upper polariton branch. (A) Angle-resolved PL spectra from a cavity sample with Δ = $-52\,meV$ detuning and $\hbar\Omega_R = 45\,meV$ showing UP emission at energies 2.44 – 2.52 eV near the cavity-exciton resonance. The lower polariton branch (2.3 - 2.41 eV) is indicated by the green line and the HH exciton energy (2.42 eV) is indicated by the red-dotted line. **(B)** Integrated linecuts of PL spectra for three different sample positions having varied zero-angle detuning. Enhanced upconverted PL for higher detuned sample positions resulting from more accessible lower-polariton states across the wider in-plane momenta range.

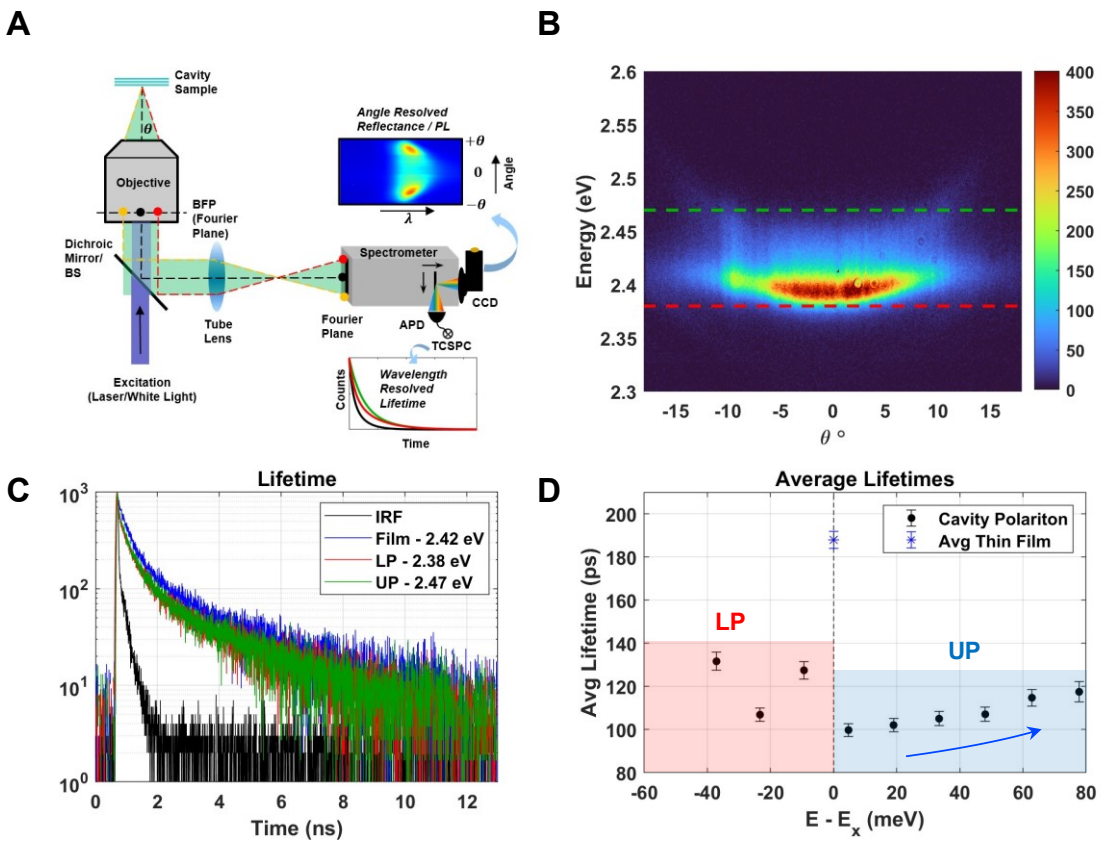

Figure 4. Energy resolved lifetime measurements of the LPB and UPB. (A) Experimental schematic showing correlated angle resolved spectroscopy with high resolution TCSPC via a dual exit port spectrometer. **(B)** Photoluminescence spectrum of a cavity sample position showing UPB and LPB emission. **(C)** Corresponding raw TCSPC lifetime curves along dotted lines in (B) and for a control half-cavity thin film sample. **(D)** Amplitude-weighted average lifetime measurements taken along every 3 nm of the emission window and converted to energy difference between the bare exciton emission and the polariton emission energy for sample position corresponding to (B). Average lifetime at peak exciton emission for a bare half-cavity thin film sample averaged along three different positions indicated by blue ∗ marker.